

Article

Accurate Modeling of Conductor Rough Surfaces in Waveguide Devices

Binke Huang *  and Qi Jia

Department of Information and Telecommunication Engineering, Xi'an Jiaotong University, Xi'an 710049, China; qqi_jia@163.com

* Correspondence: bkhuang@mail.xjtu.edu.cn; Tel.: +86-138-9195-5673

Received: 16 January 2019; Accepted: 25 February 2019; Published: 1 March 2019



Abstract: To address the effects of surface roughness on wave propagation in the microwave and millimeter-wave bands, this paper studies electromagnetic wave propagation and focuses on the propagation loss within an inner environment featuring surface roughness of the metallic waveguide structures. The conductivity gradient model is first developed to treat surface roughness with inhomogeneous conductivity, and then the concept of a frequency-dependent effective conductivity is introduced to model the effects of surface roughness in waveguide structures. With the effective conductivity used in the commercial 3D field solver, High Frequency Structure Simulator (HFSSTM), a surface impedance boundary condition strategy is applied on ideally smooth surfaces to model the actual behavior of rough metallic waveguide surfaces. Finally, the propagation performance is predicted by comparing the effects of surface roughness in metallic waveguide structures and the results from the models with ideally smooth surfaces, using rectangular waveguide, cylindrical resonator and coupling cavity filters models. Overall, this effective conductive concept can be applied using various commercial field solvers to handle surface roughness effects accurately and efficiently in any work involving conducting microwave structures.

Keywords: surface roughness; effective conductivity; waveguide structures; conductor loss

1. Introduction

Waveguides are a basic component in radar and communication applications [1–3]. The accurate modeling of electromagnetic wave propagation is an important problem, especially as majority of present and future radar and communication systems operate at higher frequencies in the millimeter-wave bands. The roughness of real physical waveguide surfaces is usually caused by either fabrication-related irregularities (caused by the material used for fabrication or the fabrication process) or environmental effects (such as corrosion). At higher frequencies, for example at the Ka band, the conductor skin depth and the root mean square (RMS) heights of the inner surface roughness are both in the micrometer range. As the skin depth would extend and fall below the dimensions of the surface roughness, the propagation losses caused by this roughness are not negligible in the accurate modeling of waveguide performance. Thus, advances in accurately modeling practical or realistic waveguide structures with finite conductivity and inner surface roughness are needed in engineering problems; this is especially important for several applications, such as in microwave measurement devices, to improve the measurement accuracy and extend the measurement range, and in high power space communication components, to improve electromagnetic reliability and operation life.

If the surface roughness must be taken into account using numerical methods, this process will involve co-simulation of multi-scale structures and will require considerable numerical effort. In 1949, Morgan [4] studied the power dissipation in a metallic plane with a rough surface at microwave frequencies using a finite difference approach. In this study, the surface roughness was modeled

as periodic grooves of various shapes and sizes; the conductor was copper with a conductivity of 5.8×10^7 S/m. Using Morgan's model, Hammerstand and Bekkadal [5] derived a widely used empirical formula that matches the numerical results produced by Morgan. This formula, given in (1), provides a correction factor describing the ratio of the power absorption of a rough surface P_{rough} to that of a corresponding smooth surface P_{smooth} .

$$K_{sr} = \frac{P_{rough}}{P_{smooth}} = 1 + \frac{2}{\pi} \tan^{-1} \left(1.4 \left(\frac{h}{\delta} \right)^2 \right), \quad (1)$$

where h is the RMS height of the rough surface profile and δ is the skin depth of the conductor. The formula given in (1) is currently the most common model that quantifies the impact of conductor surface roughness on Ohmic losses; this formula has been integrated in commercial field solvers, such as Ansys' High Frequency Structure Simulator (HFSSTM) ([Online]. Available: <http://ansoft.com/maxwell/>). However, the correction factor saturates at a value of two and therefore fails to model effects at high frequencies (small δ) or high value of RMS h , since it can be shown that the additional loss can easily exceed the value of two with measurement results [6]. The study of conductor surface roughness has attracted significant interest in planar transmission lines and interconnects on high-speed circuits. Guo et al. [7] introduced a periodic model to calculate the equivalent roughened conductor surface impedance that can then be used to modify the per-unit-length transmission line parameters to evaluate signal attenuation and phase delay. Koledintseva et al. [8] proposed a model to substitute the conductor surface roughness of printed circuit boards by a layer with an effective material (lossy dielectric) for numerical simulations. A few parameters of the model, as statistical values, can be estimated from Scanning Electron Microscope (SEM) images of the roughened surfaces. Tsang et al. [9] characterized the rough surface by a stochastic random process for high-speed interconnects and microelectronic packages. In their study, the models of the rough interface between the dielectric and conductive mediums and the rough parallel plate waveguide were investigated using an analytical second-order small perturbation method (SPM2), as well as numerical methods, such as the method of moments (MoM) and the transfer matrix (T-matrix) method. Unfortunately, these models cannot be extended straightforwardly for the models of non-TEM waveguide structures with inner surface roughness. For waveguide structures, Huang et al. [10] investigated the field distribution and cutoff frequency of a rectangular waveguide with surface roughness by using the method of moment rigorously, while the waveguide walls were modeled as perfect conductors. Ozgun et al. [11] employed transformation-based media for analyzing waveguides with grooves or rough surfaces, thereby improving the computational performance of the finite element method by eliminating the need for mesh generation at each realization corresponding to a different shape of the surface when using a Monte Carlo technique. However, the finite conductivity boundary in the transformation electromagnetics method has not yet been developed to account for the effects of rough surfaces on conductor loss. Lukic et al. [12] studied the effects of periodic 3-D surface roughness on the complex propagation constant of rectangular μ -coaxial lines using the commercial finite-element method software, HFSSTM. Importantly, direct solving for the field inside the rough conductor in the realistic recta-coax line is impractical due to the excessive memory requirements needed to accurately mesh the interior of the metal walls.

If surface roughness is modeled at a microscopic level using several intrinsic parameters (e.g., the shape of the assumed structures), it will be expected that the modeling will still differ from reality as the model assumes regular structures rather than a random and irregular surface topology. In addition, it is very likely that significant computational effort will be required for co-simulation of multi-scale structures. Recently Gold et al [13–16] proposed the conductivity gradient model to model the influence of rough surfaces in PCB transmission lines and waveguides. A frequency-dependent effective conductivity was introduced in a smooth surface conductor to account for surface roughness

effects, and this conductivity could easily be integrated into 2D/3D field solvers as a surface impedance boundary condition.

In this paper, the effective conductivity concept is employed to analyze metal-based waveguide structures and the effects of inner surface roughness. In Section 2, the conductivity gradient model for rough surfaces is described. Then, the associated Maxwell equations are solved with an inhomogeneous distribution of conductivity filled in the space. Thus, the frequency dependent effective conductivity is derived with the equivalent of conductor loss and can then be straightforwardly integrated into the surface impedance boundary condition and analyzed using the commercial 3-D software, HFSS™. In Section 3, three typical and widely used models (rectangular waveguide, cylindrical resonator, and a four pole aperture couple filter) with inner rough surfaces are investigated at millimeter wave frequencies, and the numerical results are compared with models that have ideally smooth surfaces. Finally, the conclusions from the analysis are presented in Section 4.

2. Theories

2.1. Conductivity Gradient Model for a Conductor Plane with Surface Roughness

The surface roughness profiles of conductors can be assumed to be irregular and random. The roughness profile of a plane can be measured using a stylus profilometer or by SEM. The roughness is usually characterized by two parameters: R_q , RMS average of the departure of the roughness profile from the mean surface line, and Λ_r the correlation length measuring the mean distance between consecutive peaks and valleys on the surface. The characteristics of the roughness parameters are dependent on the manufacturing process. In waveguide structure fabrication, the RMS surface roughness parameter (R_q) of the inner surface is typically in the order of $1\mu\text{m}$. For the frequencies of interest, for example at 5 GHz, the skin depth in copper is $0.93\mu\text{m}$. As this skin depth is comparable to the surface roughness parameter, the roughness effects on signal propagation in waveguides cannot be neglected.

The sizes of waveguide components are usually comparable with the signal wavelength, and the components are operated on the resonance region corresponding to the signal frequency. On the other hand, the sizes of the surface roughness are in the microscopic scale and much smaller than the component sizes. If the conductor surfaces on the component are modeled accurately by fine discretization, the numerical technique will inherently handle the fields above and in the conductors but would make the computing effort so large that it would be almost impossible to solve these multi-scale structures. In fact, since the wavelength is much greater than the scale of the RMS surface roughness R_q and the correlation length Λ_r , it is not necessary to model the microscopic features of surface roughness directly.

For an air-metal plane interface, the conductor occupies the top half space, as shown in Figure 1. Considering that the conductor and air are separated by the conductor surface profile, the conductivity around the interface is non-homogeneous. Thus, the transition from air to conductor can be quantitatively modeled as a conductivity gradient perpendicular to the surface along the y -axis direction (See Figure 1). For a random surface roughness, the surface profile height can be characterized with a probability density function (PDF), where the conductivity distribution can be expressed through the cumulative distribution function (CDF) as follows:

$$\sigma(y) = \sigma_{bulk} \cdot CDF(y) = \sigma_{bulk} \int_{-\infty}^y PDF(u) du, \quad (2)$$

where σ_{bulk} is the metal bulk conductivity and $PDF()$ is the probability density function of the surface profile height. Usually the PDF has a normal distribution due to the manufacturing process and can be obtained by measurement. Naturally, the normal distribution can be expressed with a mean value

and standard deviation. With the RMS value R_q for the conductor surface roughness, the conductivity distribution in space based on this normal distribution can be derived as

$$\sigma(y) = \sigma_{bulk} \cdot \frac{1}{R_q \sqrt{2\pi}} \int_{-\infty}^y e^{-\frac{u^2}{2R_q^2}} du. \tag{3}$$

In addition, surface profiles other than the normal distribution also are suitable to be modeled with the CDF directly. With the conductivity gradient model, we transfer the conductor surface roughness topology to a location dependent conductivity filled in space. Then, the resulting problem involves solving Maxwell’s equations for the model with an inhomogeneous conductivity distribution.

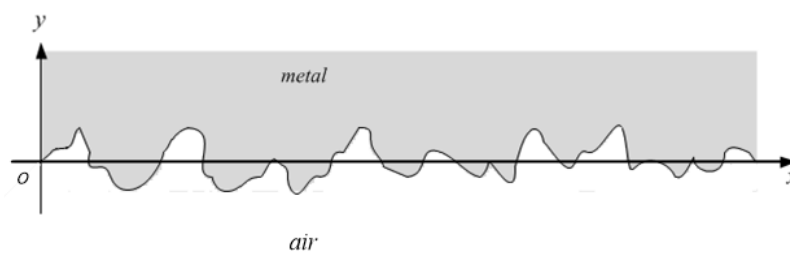


Figure 1. Profile of an air-metal plane interface with conductor surface roughness.

2.2. Field Solutions for Conductivity with Inhomogeneous Distribution in Space

In Section 2.1, the conductivity distribution for the surface roughness metal model was obtained. Based on this result, the field solutions from Maxwell’s equations for conductivity with an inhomogeneous distribution can be derived. Here, the time dependence of the form $\exp(j\omega t)$ is assumed for the time-harmonic fields and is omitted for brevity. The two Maxwell curl equations are as follows:

$$\nabla \times \bar{H} = j\omega\epsilon_0\bar{E} + \bar{J}, \tag{4}$$

$$\nabla \times \bar{E} = -j\omega\mu_0\bar{H}. \tag{5}$$

For the surface roughness conductor model shown in Figure 1, $\bar{J} = \sigma\bar{E}$. By solving Maxwell’s equation, it should be possible to obtain the magnetic field distribution \bar{H} . Taking the curl of (4), inserting Faraday’s law (5) to eliminate the electric field \bar{E} , and imposing the condition $\nabla \cdot \bar{H} = 0$, we have

$$\nabla^2\bar{H} + k_0^2\bar{H} + \nabla \times (\sigma\bar{E}) = 0, \tag{6}$$

where $k_0 = \omega\sqrt{\mu_0\epsilon_0}$. Since σ varies with y and $\bar{E} = \frac{\nabla \times \bar{H}}{j\omega\epsilon_0 + \sigma}$ from (4), the curl of the conduction current density can be calculated as

$$\nabla \times (\sigma\bar{E}) = \sigma\nabla \times \bar{E} - \bar{E} \times \nabla\sigma = -j\omega\mu_0\sigma\bar{H} + \frac{1}{j\omega\epsilon_0 + \sigma} \nabla\sigma \times \nabla \times \bar{H}. \tag{7}$$

Substituting (7) into (6), the unknown magnetic field \bar{H} is left, and (6) can be modified as:

$$\nabla^2\bar{H} + (k_0^2 - j\omega\mu_0\sigma)\bar{H} + \frac{1}{j\omega\epsilon_0 + \sigma} \nabla\sigma \times (\nabla \times \bar{H}) = 0. \tag{8}$$

Despite a location dependent $\sigma(y)$ around the air-conductor interface, the displacement current density is much smaller than the conduction current density with $\omega\epsilon_0 \ll \sigma$. Hence, the displacement current can be neglected and (8) can be approximated as

$$\nabla^2\bar{H} - j\omega\mu_0\sigma\bar{H} + \frac{\nabla\sigma}{\sigma} \times (\nabla \times \bar{H}) = 0. \tag{9}$$

It should be noted that $\sigma(y)$ will gradually transition to bulk conductivity in the direction perpendicular to the mean surface of the air-conductor rough interface. In addition, the magnetic field strength will decrease exponentially in the $+y$ direction and becomes a one dimension problem. Considering the conductor boundary shown in Figure 1, the magnetic field H_x decreases quickly with the increase of σ in the y - direction; while in the x - and z - directions, this change is less and the partial derivative in these two directions vanish in the Laplacian and curl terms of the equation (9). The H_x component can be solved from (9) as:

$$\frac{\partial^2 H_x}{\partial y^2} - j\omega\mu_0\sigma H_x - \frac{1}{\sigma} \frac{\partial\sigma}{\partial y} \frac{\partial H_x}{\partial y} = 0. \quad (10)$$

In (10), the conductivity is location dependent as $\sigma(y)$ derived from the CDF function. This equation can be efficiently solved using numerically techniques [17]. This process will yield the numerical magnetic field solution around the surface roughness and inside the conductor, and then the current density and conductor loss can be obtained directly.

2.3. Frequency Dependent Effective Conductivity for Conductor Surface Roughness

From the analysis presented earlier, field solutions have been obtained for conductor surface roughness in space using a gradient conductivity model. However, the gradient conductivity model cannot be directly employed in 3D commercial field solvers for the simulation of complex metal-based waveguide components, because the conductivity has an inhomogeneous distribution perpendicular to the mean plane of the surface roughness. In Figure 1, the conductivity increases gradually in the y -direction and exhibits bulk conductivity where the space is fully occupied by the conductor. As the field components around the air-metal rough interface space have been solved in Section 2.2, the time averaged conductor loss power density can be calculated easily with formula (4) as follows [18]:

$$P_{rough}(y) = \frac{1}{2} \frac{|\bar{J}_{rough}|^2}{\sigma(y)} = \frac{1}{2} \frac{|\nabla \times \bar{H}|^2}{\sigma(y)}. \quad (11)$$

Figure 2 shows the conductivity profile of copper ($\sigma_{bulk} = 5.8 \times 10^7$ S/m) and the loss power density distribution in an air-metal plane with surface roughness. This can then be compared with the performance of an ideal or perfectly smooth surface in Figure 2. It should be noted that both cases are normalized to the loss power density for a smooth surface at $y = 0$. It can be seen from Figure 2 that the conductor loss density first increases when the signal enters the surface roughness conductor domain. However, as the depth that the signal enters increases, the signal attenuates quickly and the conductor loss density decreases accordingly afterwards.

In order to transform the surface roughness to a smooth one for simulation with commercial field solvers, the frequency-dependent effective conductivity of a conductor with an equivalent smooth surface is defined. This can be obtained in terms of the equivalent relations of the conductor loss for the roughness surface and equivalent smooth surface models as follows

$$\int P_{rough}(y, \omega) dy = \int P_{e,smooth}(y, \omega) dy \quad (12)$$

where $\int P_{rough}(y, \omega) dy$ is the conductor loss from the surface roughness model, which can be directly calculated with (11) using numerical integration. The conductor loss for the equivalent smooth surface model can then be expressed as [18]

$$\int P_{e,smooth}(y, \omega) dy = \int \frac{1}{2} \frac{|\bar{J}_{e,smooth}|^2}{\sigma_{eff}(\omega)} dy \quad (13)$$

where $\bar{J}_{e,smooth} = \sigma_{eff} \bar{E}_{eff} = \nabla \times \bar{H}_{eff} \propto e^{-(1+j)y/\delta_{eff}}$. Thus, in summary, the calculation of the effective conductivity for an equivalent smooth surface can be obtained using (11), (12) and (13). This effective conductivity is frequency dependent and can be used to characterize the effects from surface roughness up to mm-wave region.

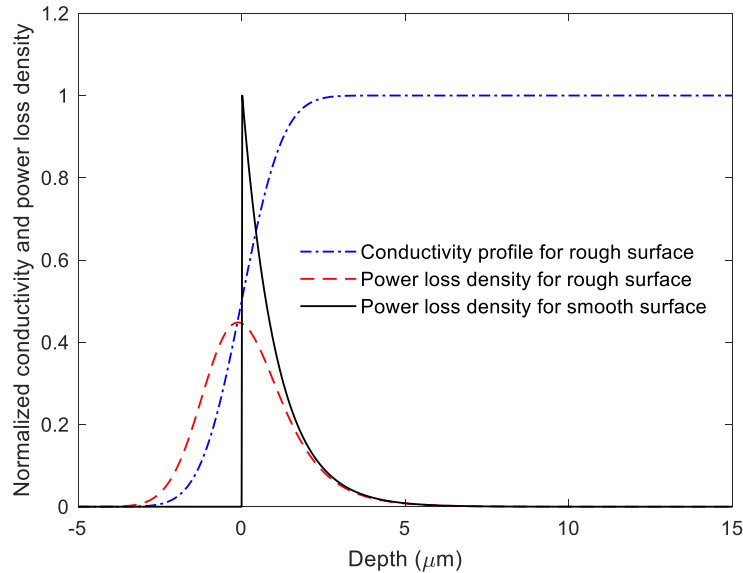


Figure 2. Profiles of the conductivity and the time averaged conductor loss power density for a surface roughness (with root mean square (RMS) value of 1 μm) and a smooth surface at 1 GHz.

The effective conductivity will be smaller than the actual bulk conductivity since the conductor loss for a surface roughness will be larger than that of the smooth surface. For conductors with a surface roughness of different RMS heights ($R_q = 0.5\mu\text{m}, 0.75\mu\text{m}, 1\mu\text{m}$), the frequency dependent effective conductivity is plotted in Figure 3, which has a good agreement with the results given in [14]. When the RMS height and frequency increases, the conductor loss increases dramatically, while the effective conductivity decreases with frequency. As shown in Figure 3, the effective conductivity is half of the DC bulk conductivity at 20 GHz with an RMS height R_q of 0.5 μm for the conductor with surface roughness, and the effective conductivity decreases even more for larger RMS height values.

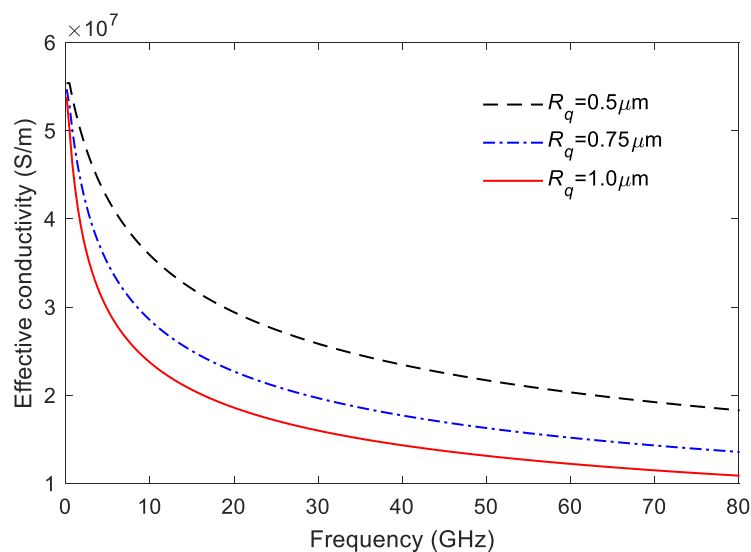


Figure 3. Frequency dependent effective conductivity for a rough surface with different values of R_q .

2.4. Surface Impedance Boundary Condition with Effective Conductivity

The electromagnetic wave attenuates exponentially when entering a conductor and the signal is concentrated only near the conductor surface within a few skin depths [19]. For metal-based waveguide components, if the air medium and conductor are both discretized with grids, the cell length will be very fine due to the rapidly varying signal inside the conductor. This will then exhaust a large amount of computer resources. Fortunately, a surface impedance boundary condition can be employed to handle the conductor boundary. For a conductor boundary in the $x - z$ plane, as shown in Figure 1, the surface impedance Z_s can be expressed as

$$Z_s = E_z/H_x = j\omega\mu_0/\gamma \quad (14)$$

where γ is the complex propagation constant in the conductor with $\gamma = (1 + j)/\delta$, and δ is the skin depth of the conductor. For conductors with a surface roughness, the equivalent frequency dependent effective conductivity σ_{eff} has been obtained. Then, the effective surface impedance is

$$Z_s = (1 + j)/(\sigma_{eff}\delta_{eff}) \quad (15)$$

where $\delta_{eff} = 1/\sqrt{\pi\mu_0\sigma_{eff}f}$ is the effective skin depth for a conductor with surface roughness. In commercial field solvers, the effective surface impedance can be incorporated to characterize the conductor boundary. Hence, it is not necessary to mesh and solve inside the conductors. Since the effective conductivity is frequency dependent, a practical approach is to import a data file containing the frequency dependent values for effective conductivity from Section 2.3 to the material library in commercial field solvers such as HFSSTM. Using the procedure outlined, the numerical simulation will be able to consider the effects of conductor surface roughness on the performance of waveguide components at high frequencies. In the following section, several examples for metal-based waveguide components will be demonstrated.

3. Examples

We proceed to study the effects of surface roughness for waveguide components with the proposed effective conductivity technique through several examples. For comparative study, the simulation results for waveguide components with a smooth surface are also provided.

The first example is a WR-28 rectangular waveguide ($a = 7.112$ mm and $b = 3.556$ mm) commonly used in space communications, where the waveguide walls are copper with a conductivity of $\sigma_{bulk} = 5.8 \times 10^7$ S/m and have an RMS value of surface roughness of 1 μ m. Figure 4a shows in a semi-logarithmic scale the attenuation constant of the first four waveguide modes as a function of the frequency. In this figure, the results for the smooth surface and the rough surface model are both implemented with the commercial software HFSSTM. For waveguide, considering finite conductivity with a smooth surface, we have achieved the simulation with HFSS software, and the results have good agreement with the perturbed boundary condition method [20]. As discussed earlier, for the surface roughness model, the effective conductivity is frequency dependent, and, consequently, a conductivity datasheet file needs to be imported into the HFSS software. It should be noted that for propagation modes above the cutoff frequencies, the conductor losses of the four modes are all noticeably increased when considering the surface roughness model. However, the cutoff frequencies for the four modes are almost not affected by the surface roughness. It should be noted that the TE₁₁ and TM₁₁ modes are degenerate and have the same cutoff frequency, while the field distributions inside the waveguide are different and accordingly have different conductor losses. Furthermore, the conductor loss for the TE₁₁ mode is larger than the TM₁₁ mode, since the field strength near the conductor boundary for the TE₁₁ mode is larger than that of the TM₁₁ mode. To decrease the conductor loss from the surface roughness, a suitable way is to reduce the field distribution of the propagating signal near the surface roughness of the waveguide. In Figure 4b, the phase constants for the first four modes are presented. On the

contrary, we can see that below the cutoff frequencies the phase constants for the surface roughness waveguide are larger than that of the smooth surface waveguide. For the propagation modes above the cutoff frequencies, the effects of surface roughness on the phase constants can be assumed to be negligible for engineering applications.

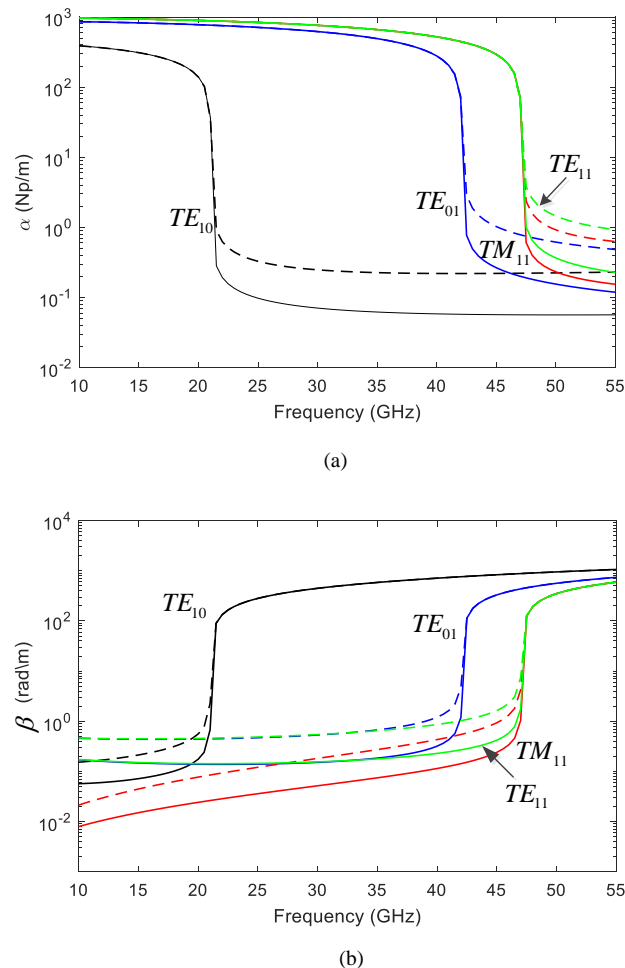


Figure 4. (a) Attenuation and (b) phase constants for the first four WR-28 rectangular modes computed with smooth surface (solid lines) and surface roughness walls (dashed lines, The lines in green color are for TE_{11} mode and the lines in red color are for TM_{11} mode).

As the second example, a cylindrical resonator that has a rough inner wall surface with a diameter of 35 mm and a height of 23.7 mm is studied. The TM_{010} , TE_{111} , and TE_{011} modes of the cylindrical resonator are analyzed with HFSSTM software simulation, and the surface roughness is characterized with the effective conductivity. The conductor wall is made of silver with a conductivity given by $\sigma_{bulk} = 6.2 \times 10^7 \text{ S/m}$ for the resonator, while the RMS value of the surface roughness is 0.6 μm . The resonance frequencies f_{rough_HFSS} and quality factors Q_{rough_HFSS} are listed in Table 1 for the three modes. For a comparative study, the results for a model with smooth surfaces from the analytical perturbation method (see (6.57) in [18]) and HFSSTM software simulation are also listed. From Table 1, we can see that resonant frequencies ($f_{smooth_analy.}$ and f_{smooth_HFSS}) and quality factors ($Q_{smooth_analy.}$ and Q_{smooth_HFSS}) have good agreement for smooth surfaces from the analytical perturbation method and HFSS simulation approach. From f_{smooth_HFSS} and f_{rough_HFSS} , we can see that surface roughness have negligible effect on the resonator frequencies but have significant effects on quality factors in comparison Q_{smooth_HFSS} with Q_{rough_HFSS} for the three modes. This indicates that the loss increase due to the surface roughness can be accurately predicted with the effective conductivity. On the other hand, resonance frequencies of resonators are influenced by the inner inductance of metals which

is related to the magnetic field response inside the conductor, the increased inner inductance can be modeled by an effective, frequency-dependent permeability $\mu_{r\text{ eff}}$ obtained by comparing the magnetic field energies of a rough and a smooth surface [13]. In addition, compared with the TM_{010} and TE_{111} modes, the field distribution for the TE_{011} mode is concentrated at the center (or axis) of the cylindrical resonator, and the fields nearly vanish around the surface roughness wall. Hence, the TE_{011} has highest quality factor among the three modes and the surface roughness may have a smaller influence on TE_{011} mode than the other two TM_{010} and TE_{111} modes.

Table 1. Resonant frequencies and quality factors of an empty cylindrical resonator.

Modes	Resonance Frequency (GHz)			Quality Factor		
	$f_{\text{smooth,analy.}}$	$f_{\text{smooth,HFSS}}$	$f_{\text{rough,HFSS}}$	$Q_{\text{smooth,analy.}}$	$Q_{\text{smooth,HFSS}}$	$Q_{\text{rough,HFSS}}$
TM_{010}	6.562	6.647	6.646	12758	12624	10041
TE_{111}	8.080	8.114	8.114	14373	14280	11129
TE_{011}	12.222	12.330	12.329	26836	26621	20757

Finally, the surface roughness effects in a four-pole filter operating in the Ka band are studied [21]. The filter is made of aluminum alloy with a conductivity equal to $1.2 \times 10^7 \text{ S/m}$. The filter is symmetrical (Figure 5) and the cavities have equal widths ($a = 8.636 \text{ mm}$) and lengths ($l_1 = 4.696 \text{ mm}$ and $l_2 = 5.555 \text{ mm}$). The cavities are made with the inductive coupling irises that have equal length ($d = 2.5 \text{ mm}$) and widths ($a_1 = 4.939 \text{ mm}$, $a_2 = 3.799 \text{ mm}$, and $a_3 = 3.578 \text{ mm}$). The RMS value of the surface roughness wall is $1 \text{ }\mu\text{m}$.

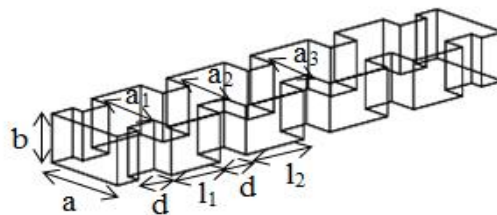


Figure 5. Structure of a four-pole inductive rectangular filter operating in the Ka band.

The filter has been designed to have a band-pass response of 800 MHz bandwidth centered at 28 GHz. A detailed view of the filter insertion losses is shown in Figure 6a, which includes the simulated results from HFSSTM, considering the finite conductivity value of the employed aluminum alloy with inner surface roughness, as well as a comparison with the result from the inner smooth surface. It can be seen that the insertion loss is larger than that of the smooth surface, especially at the high frequencies of the pass band. Moreover, at the center frequency, the insertion loss increases by about 0.6 dB for the surface roughness. The complete reflection and transmission responses of this filter are shown in Figure 6b. It can be observed that there are slight differences between the two simulated results for insertion loss and bandwidth from the two models of the smooth and rough surfaces. However, for higher frequencies (microwave and millimeter waves), accurately modeling the effects of surface roughness on increasing the insertion loss and shifting the bandwidth are essential for engineering applications, such as microwave measurement and space communication. Considering manufacturing and fabrication factors, accurate modeling of surface roughness in microwave and millimeter components will bridge the gap between the simulation and measurement results.

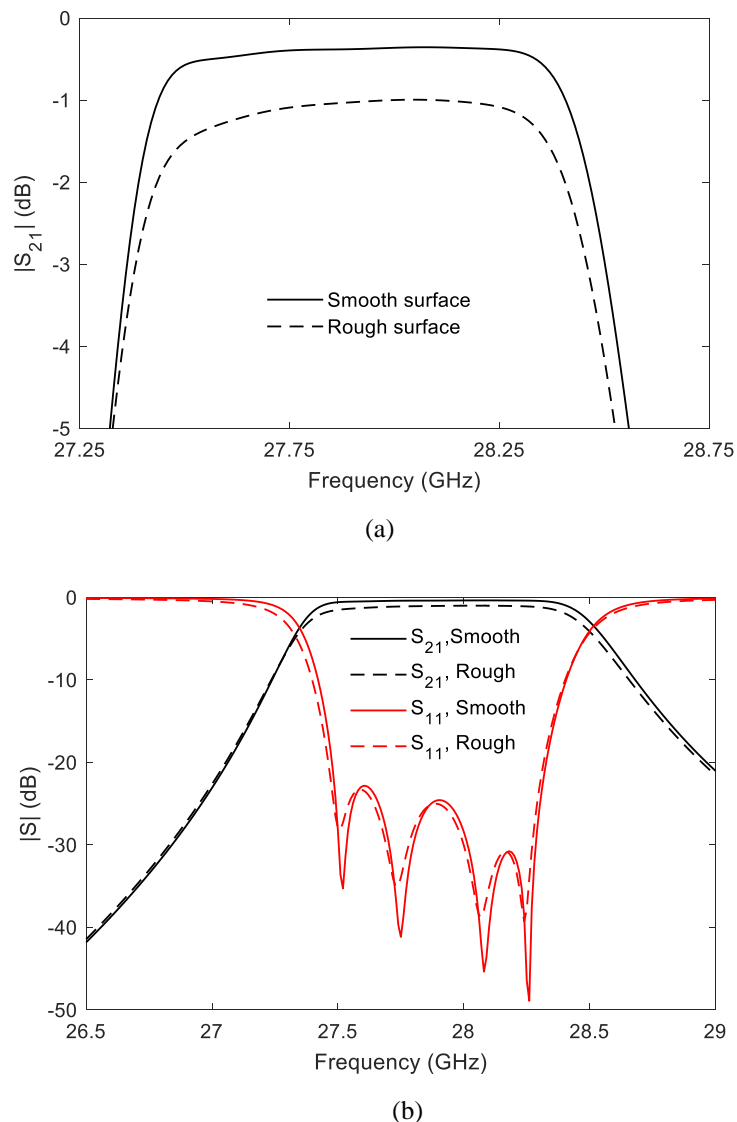


Figure 6. (a) Detailed views of the insertion losses of the four-pole filter with smooth and rough surfaces, (b) Magnitude of the scattering parameters of the four-pole inductive filter with smooth and rough surfaces.

4. Conclusions

The gradient model and effective conductivity are introduced to model the effects of conductor surface roughness in metal-based waveguide components. The frequency dependent values for effective conductivity can be easily and efficiently integrated within commercial 3D field solvers to account for surface roughness. From the comparative study with the smooth surface, the increased conductor loss due to surface roughness for waveguide components is investigated accurately. To alleviate the conductor loss from the surface roughness, a suitable method is to reduce the field strength of the propagating signal near the rough conductor walls of the waveguide [22]. For future work, the correlation length of the real random manufactured surface roughness should be taken into account to model the conductivity gradient. In addition, in the sub-millimeter and THz band, defining conductor parameters with dispersive effects in numerical simulations is a challenge for accurately modeling surface roughness in metal-based THz waveguides.

Author Contributions: B.H. developed the theory, surface roughness characterization, and wrote the paper. Q.J. performed the waveguide devices simulations with software.

Funding: This work was supported in part by the National Natural Science Foundation of China (Grant No. 61471293) and the China Scholarship Council (Grant No. 201706285142).

Conflicts of Interest: The authors declare no conflicts of interest.

References

1. Leal-Sevillano, C.A.; Cooper, K.B.; Decrossas, E.; Dengler, R.J.; Ruiz-Cruz, J.A.; Montejo-Garai, J.R.; Chattopadhyay, G.; Rebollar, J.M. Compact duplexing for a 680-GHz radar using a waveguide orthomode transducer. *IEEE Trans. Microw. Theory Tech.* **2014**, *62*, 2833–2842. [[CrossRef](#)]
2. Han, G.-D.; Du, B.; Wu, W.; Yang, B. A novel hybrid phased array antenna for satellite communication on-the-move in Ku-band. *IEEE Trans. Antennas Propag.* **2015**, *63*, 1375–1383. [[CrossRef](#)]
3. Arnold, C.; Parlebas, J.; Zwick, T. Reconfigurable waveguide filter with variable bandwidth and center frequency. *IEEE Trans. Microw. Theory Tech.* **2014**, *62*, 1663–1670. [[CrossRef](#)]
4. Morgan, S.P. Effects of surface roughness on eddy current losses at microwave frequencies. *J. Appl. Phys.* **1949**, *20*, 352–362. [[CrossRef](#)]
5. Hammerstad, E.O.; Bekkadal, F. *Microstrip Handbook*; Norwegian Institute of Technology: Trondheim, Norway, 1975; pp. 4–8.
6. Huray, P.G.; Oluwafemi, O.; Loyer, J.; Bogatin, E.; Ye, X. Impact of copper surface texture on loss: A model that works. In Proceedings of the DesignCon 2010, Santa Clara, CA, USA, 1–4 February 2010; pp. 462–483.
7. Guo, X.; Jackson, D.R.; Koledintseva, M.Y.; Hinaga, S.; Drewniak, J.L.; Chen, J. An analysis of conductor surface roughness effects on signal propagation for stripline interconnects. *IEEE Trans. Electromag. Compat.* **2014**, *56*, 707–714. [[CrossRef](#)]
8. Koledintseva, M.; Koul, A.; Zhou, F.; Drewniak, J.; Hinaga, S. Surface impedance approach to calculate loss in rough conductor coated with dielectric layer. In Proceedings of the 2010 IEEE International Symposium on Electromagnetic Compatibility, Fort Lauderdale, FL, USA, 25–30 July 2010; pp. 790–795.
9. Tsang, L.; Braunisch, H.; Ding, R.; Gu, X. Random rough surface effects on wave propagation in interconnects. *IEEE Trans. Adv. Packag.* **2010**, *33*, 839–856. [[CrossRef](#)]
10. Huang, B.-K.; Chen, J.; Jiang, W.-S. Effects of surface roughness on TE modes in rectangular waveguide. *J. Infrared Millim. Terahertz Waves* **2009**, *30*, 717–726. [[CrossRef](#)]
11. Ozgun, O.; Kuzuoglu, M. Transformation electromagnetics based analysis of waveguides with random rough or periodic grooved surfaces. *IEEE Trans. Microw. Theory Tech.* **2013**, *61*, 709–719. [[CrossRef](#)]
12. Lukic, M.V.; Filipovic, D.S. Modeling of 3-D surface roughness effects with application to μ -Coaxial lines. *IEEE Trans. Microw. Theory Tech.* **2007**, *55*, 518–525. [[CrossRef](#)]
13. Gold, G.; Helmreich, K. A physical surface roughness model and its applications. *IEEE Trans. Microw. Theory Tech.* **2017**, *65*, 3720–3732. [[CrossRef](#)]
14. Gold, G.; Helmreich, K. Effective conductivity concept for modeling conductor surface roughness. In Proceedings of the DesignCon 2014: Where the Chip Meets the Board, Santa Clara, CA, USA, 28–31 January 2014; pp. 1–21.
15. Gold, G.; Helmreich, K. A physical model for skin effect in rough surfaces. In Proceedings of the 42nd European Microwave Conference, Amsterdam, The Netherlands, 29 October–1 November 2012; pp. 1011–1014.
16. Lomakin, K.; Gold, G.; Helmreich, K. Analytical waveguide model precisely predicting loss and delay including surface roughness. *IEEE Trans. Microw. Theory Tech.* **2018**, *66*, 2649–2662. [[CrossRef](#)]
17. Press, W.H.; Teukolsky, S.A.; Vetterling, W.T.; Flannery, B.P. *Numerical Recipes in FORTRAN-The Art of Scientific Computing*, 2nd ed.; Cambridge University Press: Cambridge, UK, 1992; pp. 704–708.
18. Pozar, D.M. *Microwave Engineering*, 4th ed.; John Wiley & Sons, Inc.: Hoboken, NJ, USA, 2011; pp. 31–34.
19. Hall, S.H.; Heck, H.L. *Advanced Signal Integrity for High-speed digital Designs*; John Wiley & Sons, Inc.: Hoboken, NJ, USA, 2009; pp. 201–206.
20. Yan, S.; Huang, B.-K.; Jiang, W.-S.; Jiang, Y.-S. Calculation of the propagation constants in waveguides with imperfect conductor by the perturbed boundary condition method. *J. Microw.* **2010**, *26*, 35–38. (In Chinese)

21. Taroncher, M.; Hueso, J.; Cogollos, S.; Gimeno, B.; Boria, V.E.; Vidal, A.; Esteban, H.; Guglielmi, M. Accurate consideration of metal losses at waveguide junctions using admittance and impedance integral equation formulations. *Radio Sci.* **2005**, *40*, RS6013. [[CrossRef](#)]
22. Ramo, S.; Whinnery, J.R.; van Duzer, T. *Fields and Waves in Communication Electronics*; John Wiley & Sons, Inc.: New York, NY, USA, 1994; p. 433.



© 2019 by the authors. Licensee MDPI, Basel, Switzerland. This article is an open access article distributed under the terms and conditions of the Creative Commons Attribution (CC BY) license (<http://creativecommons.org/licenses/by/4.0/>).